Supplemental Materials

Molecular Biology of the Cell

Zaytsev and Grishchuk

Basic mechanism for biorientation of mitotic chromosomes is provided by the kinetochore geometry and indiscriminate turnover of kinetochore microtubules

Anatoly V. Zaytsev[a] and Ekaterina L. Grishchuk[a]

[a] Department of Physiology, Perelman School of Medicine, University of Pennsylvania, Philadelphia, PA 19104

Supplemental Information

Supplement 1. Model description

1.1 General framework and simplifications

Here we use a highly simplified model of kinetochore-microtubule (MT) interactions. The model contains dynamic MTs, which grow from two spindle poles in random directions, one pair of sister chromatids and a cell boundary (Figure 1A). Spindle and MT parameters are chosen based on literature and they reproduce realistically the frequency of MT binding to the kinetochore and enable taking into account the MT-dependent and thermal rotations of metaphase kinetochores. Detailed consideration of the motions and orientations of sister kinetochores is based on Langevin equations of motion in viscous medium. We also consider the realistic kinetochore geometry, number of kinetochore MTs (KMTs) and examine the physiological range of detachment frequencies (KMT turnover). This modeling framework permits a systematic and quantitative analysis of the impact of KMT turnover and kinetochore geometry on the accuracy of chromosome segregation. However, many other aspects of the MT-based mitotic spindle in our model are highly simplified, so this modeling framework is not suitable for describing other aspects of mitotic physiology, including detailed chromosome kinematics during congression.

Most significant model simplifications:

a) Each simulation was carried out for one pair of sister chromatids positioned either randomly within the cell boundary or midway between two poles. To simulate mitosis in cells with numerous chromosomes multiple simulations were performed with one such pair. This simplification can potentially affect the kinetics of "search and capture" of chromosome by the MTs (Wollman *et al*., 2005; Magidson *et al*., 2011). In our model, however, this effect is compensated via several model features, as described in Supplement 3.1. This simplification is not expected to affect kinetochore behavior in metaphase and the steady-state outcomes of our simulations.

b) Chromosomes move directionally only under the forces generated from the depolymerizing MT plus-ends. To avoid steric clashes, during initial poleward motion the kinetochore pair is not allowed to move closer than 1 μm to a spindle pole. In real cells the kinematics of chromosome motion is more complex and chromosomes move under various forces, generated by kinetochore-localized motor proteins, polar wind and chromokinesins (reviewed in Walczak *et al*., 2010). However, after the K-fiber forms and chromosome aligns at metaphase plate, the behavior of the chromosomes is determined largely by the dynamics of KMTs. In the model chromosome motion along spindle axis is restricted within 1 μm segment at the spindle equator to mimic chromosome alignment. This was done by monitoring the absolute coordinate of a chromosome moving along spindle axis (with zero at the spindle mid-point); when the coordinate became > 1 μm, the coordinate value from the previous iteration was assigned instead.

c) To speed up calculations we reduced space dimensionality to quasi-two dimensions (2D), as described in Supplement 1.2 section f, below.

d) For simplicity, the rate of KMT turnover did not change during a mitotic simulation. In real cells, the half-life of KMT attachments changes as cell progresses from prometaphase to metaphase (Zhai *et al*., 1995; Kabeche and Compton, 2013). To estimate the contribution from such a change, we compared the results for simulation with the constant turnover rate and when KMT lifetime changed from 3 to 6 min at 20 min from the start of simulations (corresponding to mitosis in PtK1 cells). Supplemental Figure S1B demonstrates that the constant turnover rate simplification does not change the steady-state model solutions and has only small effect on the modeled kinetics.

1.2 Model description

a) Formation of the mitotic spindle. At the beginning of simulations, spindle poles were positioned close to each other and ~2 μm away from the top cell boundary. To mimic spindle formation, pole motion was simulated along the pre-defined elliptic trajectory near cell boundary until the pole-to-pole distance reached 10 μm, as in mammalian cells (Mastronarde *et al*., 1993; Giodini *et al*., 2002). Pole separation motion lasted 2 min (Toso *et al*., 2009), after which the pole positions were fixed for the duration of simulation. To mimic monastrol-washout experiments, spindle poles separation was delayed by 5 min from the beginning of simulations. During this period both poles nucleated MTs, which interacted with a kinetochore pair. At 5 min spindle poles started to separate with the speed and trajectories identical to those in regular simulations (Supplemental Video 5).

b) MT nucleation and dynamics. We assume that each pole can nucleate about 750 MTs (McIntosh and Landis, 1971). Polymerization of MT was initiated from the pole in a random direction. MT dynamics parameters were chosen based on data for mitotic mammalian cells (Rusan *et al*., 2001). MT switched into depolymerization if its growing end reached the cell boundary. After MT has depolymerized completely, the new MT growth was initiated from the same pole in a random direction.

c) Sister chromatids and kinetochores geometry. Sister chromatids were simulated as two rigid semi-cylinders with the radius 0.3 μm, connected by a linear spring with rigidity k_{kin} and resting length L_k. The resting length is assumed to be 0.8 μm, which is similar to the distance between sister kinetochores in the absence of KMTs (Loncarek *et al.*, 2007; Wan *et al*., 2009). The kinetochore in the model could bind up to 45 KMTs, based on the maximal experimentally observed number of KMTs per kinetochore in PtK1 cells (McEwen *et al*., 1997). For human cells, the maximal occupancy is 24 (Wendell *et al*., 1993; McEwen *et al*., 2001). Mitotic kinetochores can be stretched up to 1.6 μm at metaphase, which corresponds to the inter-kinetochore spring elongation of 0.8 μm, giving the rigidity of inter-kinetochore spring k_{kin} = 45 pN × 25 / 0.8 μm = 1.4 pN/nm, where 45 pN is the estimated maximal force generated by a single MT (Grishchuk *et al*., 2005) and 25 is the average number of KMTs at metaphase in PtK1 cells (McEwen *et al*., 1997).

d) Force-velocity relationship for the KMTs. We assume that force $\boldsymbol{F}$, generated by a single depolymerizing MT depends linearly on the velocity of its plus-end $\boldsymbol{V}$. This relationship can be expressed with the following vector equation:

$$\boldsymbol{F} = \boldsymbol{R}\,(A + b\,(\boldsymbol{R}, \boldsymbol{V})) \qquad (s1)$$

where ***R*** is a unit vector from the MT plus-end to the corresponding pole and (***R***, ***V***) is the scalar product of ***R*** and ***V***. Parameter A, corresponding to the maximal force generated by the disassembling MT (velocity is zero), was set to 45 pN. Parameter b was estimated from the velocity of depolymerization V_{dep} of a free MT plus-end at zero force: 45/14.1 = 3.2 pN min/μm.

e) Chromosome diffusion coefficient (D_{chrom}). To estimate diffusion coefficient of mammalian chromosome we used relationship observed between the diffusion coefficient of a particle in cytoplasm and its molecular mass (Mastro and Keith, 1984). By extrapolating to the estimated chromosome molecular mass (10^8 Da; Wray *et al*., 1972) we obtain $D_{chrom} = 10^{-11}$ cm^2/s. Viscosity coefficient for the chromosome γ = 0.006 pN s/nm was taken from (Nicklas, 1965).

f) 2D representation of the 3D model. To speed up calculations we generated a quasi-two dimensional representation of our full model by building a plane through the centers of two poles and the center of symmetry of the chromosome, and then selecting a layer with thickness h_{kin} around this plane (Supplemental Figure S1C). Thickness h_{kin} was 0.5 μm, similar to the size of the kinetochore in mammalian cells (Alexander and Rieder, 1990). Importantly, because both poles are included in this layer, forces acting on the chromosome from the depolymerizing KMTs are also confined to this layer (blue and red arrows in Supplemental Figure S1C). Therefore, trajectory of chromosome motion under these forces also belongs to the selected layer. We then estimated a fraction of the MTs included in this layer (green lines in Supplemental Figure S1C) from the total number of MTs generated by a pole (grey lines in Supplemental Figure S1C); it is given by ~ h_{kin} / ($d \times \pi$) where d is the pole-to-kinetochore distance (Supplemental Figure S1D). Averaging d from 1 to 5 μm, the range of distances between the kinetochore and pole, we obtain coefficient ~ 0.06, which corresponds to 0.06 × 750 = 45 MTs per pole in 2D model.

Next, we examined how chromosome rotations affect the results of simulations with the 2D model. In cells, a chromosome can rotate in 3D volume, so this motion can be decomposed into 3 separate rotations around each axis (X, Y and Z; Supplemental Figure S1C inset). Rotations around each of these axes change the kinetochore area that is accessible for binding by the MTs growing from the pole that this kinetochore is facing, but the effects from different axes are different. Rotations around Z-axis, which lies within the layer, are calculated in our quasi-2D model explicitly, so no additional adjustment is necessary. Rotations around Y-axis can reduce the MT-binding area, because small areas of the kinetochore plate may become excluded from the layer. We estimate that this effect does not exceed 10%, so we disregard this difference. However, rotations around X-axis could not be ignored because they significantly reduce the kinetochore's accessibility for MTs. Moreover, mammalian kinetochores have been reported to be located in the ~0.3 μm deep pits, formed by the surrounding chromatin (Alexander and Rieder, 1990; Roos, 1973); such geometry further reduces the MT accessibility during X-axis rotations (Supplemental Figure S1E). To estimate this effect we simulated N=256 random chromosome orientations with kinetochore located in such a pit and calculated the kinetochore area that was accessible for MT binding: this area was 3-times smaller than the full kinetochore area, implying that only a third of the kinetochore could interact with MTs within the selected layer. To account for X-rotations in the simplified 2D model we therefore assumed that the maximal kinetochore

occupancy was ~ 33%, i.e. 15 KMTs for PtK1 cells and 8 KMTs for human cells. The number of KMTs obtained in 2D calculations was multiplied by 3 before depicting these data with graphs, such that these theoretical results could be compared directly with experiment.

g) Other modeling terminology and procedures. We define the "biorientation time" as the time required to reach 95% of the steady-state level for chromosome biorientation. The "steady-state" results were obtained in simulations lasting 3 h each. Our model does not consider the events of anaphase. To evaluate how merotelic attachments affect chromosome lagging and mis-segregation in anaphase we extracted from the model the frequency of different merotelic configurations (number of merotelic KMTs and M/A ratio) found at fixed times from the beginning of the simulations. Then, different assumptions were applied about whether these configurations cause lagging and/or mis-segregation, as described in the main text.

1.3 Kinetochore-microtubule interactions

In the model with geometric constraints, if a growing MT plus-end encounters the non-binding surface of a kinetochore pair, it immediately starts disassembling. If a growing MT plus-end encounters kinetochore corona, it also switches into disassembly but generates a pulling force on this kinetochore. In the model with KMT turnover, the attached KMT can detach with the detachment rate k_{det}, after which it becomes a free MT plus-end and starts depolymerizing. This turnover is characterized by the KMT half-life time $\tau_{1/2}$, which is the-time required for half of the KMTs to detach. KMT detachment rate k_{det} is linked with the KMT half-life $\tau_{1/2}$ with the following equation:

$$k_{\mathrm{det}} = \frac{\ln 2}{\tau_{1/2}} \qquad \text{(s2)}$$

Different rates of KMT turnover were simulated in the model by varying parameter k_{det}. In simulations that mimic permanent KMT attachments (no KMT turnover), k_{det} was set to 0.

1.4 Equations of chromosome motions under the MT pulling force

Movement of a chromosome was described in terms of Newtonian dynamics. Force from a depolymerizing MT induced directed movement in 2D layer (described as a motion of the center of chromosome mass) and it changed the orientation of kinetochore pair (described as a rotation around the center of chromosome mass). Kinetochore axis was defined as a line connecting the centers of sister kinetochores (Figure 1C). The force vector applied to the kinetochore pair from a single KMT is shown in Supplemental Figure S2A ($\boldsymbol{F_i}$); the equations of motion for the chromosome under the forces from multiple KMTs in viscous environment are written below:

$$\gamma \boldsymbol{V_c} = \sum_{i=1}^{N_{MT}} \boldsymbol{F_i} \qquad\qquad \eta\, \boldsymbol{\omega} = \sum_{i=1}^{N_{MT}} \boldsymbol{M_i} \qquad \text{(s3)}$$

where γ and η – coefficients of viscous friction for translational and rotational motions, respectively; $\boldsymbol{V_c}$ and $\boldsymbol{\omega}$ – translational and angular velocities of the chromosome, respectively; $\boldsymbol{F_i}$ and $\boldsymbol{M_i}$ – force and torque produced by a pulling KMT with index i, respectively; N_{MT} – number of attached MTs.

The velocity of KMT attachment point $\boldsymbol{V_i}$ is a sum of the translational velocity of the center of mass of the chromosome $\boldsymbol{V_c}$ and the angular velocity of the chromosome $\boldsymbol{\omega}$ relative to its center of mass:

$$\boldsymbol{V_i} = \boldsymbol{V_c} + [\boldsymbol{\omega}, \boldsymbol{r_i}] \tag{s4}$$

where $\boldsymbol{r_i}$ is the vector from the center of mass of the chromosome to the KMT attachments point on the chromosome; $[\boldsymbol{\omega}, \boldsymbol{r_i}]$ is the vector product of $\boldsymbol{\omega}$ and $\boldsymbol{r_i}$. The torque ($\boldsymbol{M_i}$) generated by attached KMT on the chromosome can be expressed as follows:

$$\boldsymbol{M_i} = [\boldsymbol{r_i}, \boldsymbol{F_i}] = [\boldsymbol{r_i}, \boldsymbol{R_i}] (A + b (\boldsymbol{R_i}, \boldsymbol{V_i})) = [\boldsymbol{r_i}, \boldsymbol{R_i}] (A + b (\boldsymbol{R_i}, \boldsymbol{V_c}) + b (\boldsymbol{R_i}, [\boldsymbol{\omega}, \boldsymbol{r_i}])) \tag{s5}$$

where A and b are coefficients (see Supplement 1.2 section d) and $\boldsymbol{R_i}$ is the unit vector codirectional with KMT. Therefore, $\boldsymbol{V_c}$ and $\boldsymbol{\omega}$ for the chromosome are given by the following system of equations:

$$\begin{aligned} \gamma \boldsymbol{V_c} &= \sum_{i=1}^{N_{MT}} \boldsymbol{R_i} (A + b (\boldsymbol{R_i}, \boldsymbol{V_c}) + b (\boldsymbol{R_i}, [\boldsymbol{\omega}, \boldsymbol{r_i}])), \\ \eta \boldsymbol{\omega} &= \sum_{i=1}^{N_{MT}} [\boldsymbol{r_i}, \boldsymbol{R_i}] (A + b (\boldsymbol{R_i}, \boldsymbol{V_c}) + b (\boldsymbol{R_i}, [\boldsymbol{\omega}, \boldsymbol{r_i}])) \end{aligned} \tag{s6}$$

Additionally, model includes thermal fluctuations, which affect kinetochore position (diffusion in 2D layer) and the length of inter-kinetochore spring, which fluctuates according to Boltzmann's distribution with temperature *T*. Energy of deformation of inter-kinetochore spring is given by:

$$E(L) = \frac{k_{kin}(L - L_k)^2}{2} \tag{s7}$$

According to Boltzmann's distribution, the probability *p* to find spring with length *L* is:

$$p \sim \exp\left[-\frac{E(L)}{k_B T}\right] = \exp\left[-\frac{k_{kin}(L - L_k)^2}{2k_B T}\right] \tag{s8}$$

where k_{kin} – rigidity of the inter-kinetochore spring, *L* – length of the inter-kinetochore spring, L_k – resting length of the inter-kinetochore spring, k_B – Boltzmann's constant, *T* – temperature.

Because pole positions at maximum separation are fixed and MTs are non-stretchable, thermal fluctuations in spring's length cannot alter the length of the MT-containing K-fibers. Instead, the kinetochore pair rotates slightly to compensate for the small changes in distance between sister kinetochores, which result from extensibility of the inter-kinetochore spring. For kinetochore-

kinetochore distance *L*, the angle between the kinetochore and spindle axes has a stochastic component (dψ) calculated as:

$$d\psi = \mathrm{Cos}^{-1}(L_k / L) \quad \text{(s9)}$$

Chromosome diffusion was represented in the model by the small stochastic terms d*x* and d*y*, applied to *x* and *y* coordinates of chromosome, respectively, at each time step:

$$dx = dy = N(0,1)\ (2\ D_{chrom}\ dt)^{0.5} \quad \text{(s10)}$$

where, N(0,1) – Gaussian distribution with mean 0 and standard deviation 1, D_{chrom} – diffusion coefficient of the chromosome and *dt* – time step.

1.5 Description of the simulation algorithm

Before start of a simulation the initial values of parameters were defined (Supplemental Figure S2B). In simulations that started with randomly positioned kinetochore pair, chromosome Y-coordinate at time t=0 was set to a random number from the range (0 μm, 3.5 μm), and the orientation angle of the chromosome was set to a random number from the range (0, π). All MTs were in "polymerization" state and their initial lengths were set to 0. Spindle poles were located at the same point with the (X,Y) coordinates (0 μm, 1.5 μm) relative to the center of the cell. For simulations that started with kinetochore pair in a favorable configuration, center of the chromosome was located at the center of the cell at t=0, and the orientation angle of the chromosome was set to 0. Left and right spindle poles had initial coordinates (-5 μm, 0 μm) and (5 μm, 0 μm) respectively. During each iteration several computational steps were performed:

Step 1. Polymerization (or depolymerization) of free MTs. The length of MTs not connected to the kinetochore was increased (or decreased) by $V_{pol}\ dt$ (or $V_{dep}\ dt$), where V_{pol} and V_{dep} were MT polymerization and depolymerization velocities, respectively.

Step 2. Change of the dynamic state of free MTs. The probability Ψ_{cat} (or Ψ_{res}) of switching to catastrophe (or rescue) for a free polymerizing (or depolymerizing) MT was calculated as given below:

$$\Psi_{cat} = f_{cat}\ dt$$
$$\Psi_{res} = f_{res}\ dt$$

here, f_{cat} (or f_{res}) was MT catastrophe (or rescue) frequency.

Next, for each free MT a random number *p* from the range [0, 1] was generated. If *p* was smaller than Ψ_{cat} (Ψ_{res}) this MT switched to depolymerization (polymerization). If *p* was larger than Ψ_{cat} (Ψ_{res}) this MT remained in the same dynamic state.

Step 3. Formation of new kinetochore-MT connections. If position of the plus-end of free MT overlapped with a corona this MT attached to the kinetochore and was subsequently called KMT. This procedure was repeated for all free MTs.

Step 4. Detachment of the KMTs. The KMT detachment probability (Ψ_{det}) was calculated as follows:

$$\Psi_{det} = k_{det}\, \mathrm{d}t$$

where k_{det} is the KMT detachment rate. Next, for each KMT a random number p from the range [0,1] was generated. If p was smaller than Ψ_{det} this KMT lost its connection to the kinetochore and became a free MT in depolymerization state. If p was larger than Ψ_{det} this MT remained connected to the kinetochore.

Step 5. Updating of chromosome position and orientation. After solving the system (s6) the velocity vector of the center of mass $\boldsymbol{V_c}$ and the projection of angular velocity ω of the chromosome were calculated. Updated coordinates of the center of the mass of the chromosome (x^{new}, y^{new}) were calculated as follows:

$$x^{new} = x^{old} + V_c^{\,x}\, \mathrm{d}t + \mathrm{d}x$$
$$y^{new} = y^{old} + V_c^{\,y}\, \mathrm{d}t + \mathrm{d}y$$

where $V_c^{\,x}$ and $V_c^{\,y}$ were the x and y projections of the vector $\boldsymbol{V_c}$ respectively; x^{old} and y^{old} were the coordinates of the chromosome at previous iteration, dx and dy were the stochastic additions representing thermal noise, see equation (s10). Then, the orientation angle of the chromosome ψ^{new} was updated:

$$\psi^{new} = \psi^{old} + \omega\, \mathrm{d}t + \mathrm{d}\psi$$

where ψ^{old} was the orientation of the chromosome at previous iteration and $\mathrm{d}\psi$ was the stochastic addition representing thermal noise, see equation (s9).

Supplement 2. Derivation of analytical equations

By definition, in the absence of geometric constraints MT from both poles can bind to a sister kinetochore with equal probabilities. We used analytical approach to calculate the resulting probability of chromosome biorientation. If kinetochore binds MTs from both poles equally well, the probability that one attached KMT is from the correct pole is 0.5. If kinetochore has N_{MT} MTs, the probability that all these MTs are correct is $(0.5)^{N_{MT}} = 2^{-N_{MT}}$. Therefore, for two sister kinetochores, the probability that both kinetochores have only correct MTs is $(2^{-N_{MT}})^2 = 2^{-2N_{MT}}$. To calculate chromosome biorientation probability, equation (1) in main text, this number was multiplied by 2 because two different configurations can lead to biorientation.

When KMT turnover is present, one needs to take into account that the number of MTs at the kinetochore (N_{MT}) is now less than the maximum possible number of MTs per kinetochore (N_{max}). To calculate the probability of biorientation (p_{bi}) in presence of KMT turnover and with no geometric constraints, we summed all possible configurations of KMT attachments for both sister kinetochores:

$$p_{bi} = \sum_{k=1}^{2N_{max}} Ocp_k \, Corr_k \qquad \text{(s11)}$$

where Ocp_k is probability that a sister kinetochore pair has only k KMTs attached from total $2N_{max}$; $Corr_k$ is probability that a sister kinetochore pair with k KMTs is amphitelic. Analytical function for Ocp_k was then derived using the following considerations. Probability that one MT was attached (regardless of whether it is merotelic or not) was (N_{MT}/N_{max}), and probability that k MTs were attached was $(N_{MT}/N_{max})^k$. Probability that all other ($2N_{max} - k$) MTs were not attached was $(1 - N_{MT}/N_{max})^{(2\,Nmax\,-\,k)}$. Therefore, analytical expression for Ocp_k can be written as:

$$Ocp_k = C(2N_{max},k)\frac{2N_{max}!}{k!(2N_{max}-k)!}\left(\frac{N_{MT}}{N_{max}}\right)^k\left(1-\frac{N_{MT}}{N_{max}}\right)^{2N_{max}-k} \qquad \text{(s12)}$$

where $C(2N_{max},k)$ is binomial coefficient to account for the number of possible combinations of k KMTs from the total occupancy $2N_{max}$. Analytical expressions for function $Corr_k$ is analogous to equation (1) derived above:

$$Corr_k = 2^{1-k}; \qquad \text{(s13)}$$

Combining (s11) with the expressions in (s12) and (s13), we write the final expression for the biorientation probability in the model with the KMT turnover and no geometric constraints:

$$p_{bi} = 2\sum_{k=1}^{2N_{\max}} \frac{2N_{\max}!}{k!(2N_{\max}-k)!}\left(\frac{N_{MT}}{N_{\max}}\right)^k\left(1-\frac{N_{MT}}{N_{\max}}\right)^{2N_{\max}-k} 2^{-k} \qquad \text{(s14)}$$

We note that with no KMT turnover $N_{max} = N_{MT}$, and equation (s14) converts to equation (1).

To calculate the biorientation probability in the presence of geometric constraints, see equation (2), we used parameter η, which describes the probability that KMT is merotelic. Probability that KMT is correctly attached is, therefore, $(1-\eta)$. For a sister kinetochore with N_{MT} KMTs, the probability that all KMTs are attached correctly is given by $(1-\eta)^{N_{MT}}$, and the biorientation probability for a kinetochore pair equals $(1-\eta)^{2N_{MT}}$ multiplied by 2 to account for two possible orientations of the bioriented

kinetochore. This expression was used to calculate data in Figure 1E, using the value of η determined from the simulations with our model.

Supplement 3. Additional model results

3.1. "Search and capture" time in the model and comparison with published theoretical models. The time to capture 46 chromosomes in our model (calculated as the longest time to capture a single chromosome after 46 repetitions, see (Wollman *et al*., 2005)) is 1.4 ± 0.2 min. This is similar to what was reported by Wollman *et al*., 2005, who used a similarly designed model which was additionally supplemented with a biased search provided by RanGTP gradient. With no biased search, Wollman *et al*., 2005 predicted a significantly longer chromosome capture time. Although our model does not include RanGTP gradient for biased MT stabilization, it has several other features that were absent in (Wollman *et al*., 2005) and which decrease the search time, explaining different model predictions. The effect of each of these factors on the time to capture the chromosomes was examined in separate calculations, and there results are reported below and in Supplemental Figure S3A.

a. Our model contains cell boundary, which upon contact causes MT to depolymerize, accelerating the capture process by 3.3-fold because it indirectly biases MT growth towards the center of the cell.

b. In our model the pole-to-pole distance is 10 μm, close to metaphase spindle length in PtK1 and human cells (Mastronarde *et al*., 1993; Giodini *et al*., 2002); this is in contrast to 20 μm spindle length used in (Wollman *et al*., 2005). Our simulations show that shortening pole-to-pole distance from 20 μm to 10 μm accelerates the capture process by 7.1-fold.

c. Random diffusion (including rotation) of the MT-free chromosome, which is included in our model, reduces the capture time by about 2.2-fold relative to the simulations in which such motions were not included. This effect is analogous to the acceleration of chromosome search due to random changes in chromosome position reported in (Paul *et al*., 2010).

d. When simulations start from the side-by-side spindle poles, the chromosome capture time is reduced 1.5-fold relative to simulations which start from the already separated poles.

Importantly, when all these factors are not included, the mean time to capture all 46 chromosomes in our model is 69 ± 26 min, similarly to time reported in (Wollman *et al*., 2005) with no biased search, so there is no contradiction between these studies. The capture time decreases dramatically to 1.4 ± 0.2 min in our model when all accelerating factors are included (Supplemental Figure S3A).

Importantly, our model was not designed to study details of the "search and capture" processes and chromosome kinematics, which would require including additional processes and features. However, the model we employ appears to provide adequate framework to study biorientation accuracy, because it realistically reproduces the angles for kinetochore-MT binding and enables taking into account the spindle and kinetochore mechanics, including the MT-dependent and thermal rotations of metaphase kinetochores. Moreover, our model recapitulates accurately the frequency of MT attachment to the kinetochore; by repeating multiple simulations we estimate that P_{at} = 3.0 min^{-1}, based on the initial slope

of the N_{MT} vs. $\tau_{1/2}$ dependency multiplied by ln2 in Supplemental Figure S3B. This value is highly similar to the frequency of MT attachment to the kinetochore estimated based on the known size of the metaphase K-fiber and the rate of MT turnover. Indeed, at steady-state the rate of MT attachment to the kinetochore (P_{at}) is same as the rate of KMT detachments, which equals $N_{MT}\ln 2/\tau_{1/2}$, where N_{MT} is the K-fiber size and $\tau_{1/2}$ is KMT half-life. For PtK1 cells, the average number of KMTs is 25 and metaphase $\tau_{1/2}$ = 6 min (Kabeche and Compton, 2013), leading to effective P_{at} = 2.9 min^{-1}. Thus, although our modeling framework is highly simplified, it contains the most important basic features and parameter values that define accuracy of KMT attachment during mitosis.

3.2. Kinetics of the formation of different types of KMT attachments. We used our model to simulate the experimental time course for kinetochore-MT attachments following monastrol washout (Supplemental Figure S3D). To enable better comparison of this theoretical time course with results of a similar experimental analysis in (Silkworth *et al*., 2012), we adjusted model behavior to better match the experimentally observed rate of spindle pole separation in that study. In these simulations, spindle poles were positioned 6 μm away from each other and MT polymerization was initiated at t = 0, imitating washout of nocodazole in (Silkworth *et al*., 2012). Pole separation was programmed to stop 10 min from the beginning of simulation, mimicking kinetics data in Figure 4D in (Silkworth *et al*., 2012). Simulations continued for additional 30 min and the fractions of kinetochores with different KMT configurations were plotted as a function of time. Since in fixed cell images a single inappropriate KMT would have been difficult to detect, when analyzing modeling results we assumed that at least 2 inappropriate KMTs must be found at theoretical kinetochores to score these configurations “merotelic” or “syntelic”. Supplemental Figure S3D demonstrates that with this assumption, the predicted evolution of different kinetochore configurations is roughly similar to the experimental time course, with the most notable difference in the abundancy of merotelic configurations. Indeed, this is one of the major results of our study that the basic mechanism alone cannot explain the experimentally observed frequency of biorientation.

Supplemental Figure legends

Supplemental Figure S1. Schematics of the model geometry.

A. Illustration of possible KMT configurations during mitosis. Red and blue lines represent KMTs from the left and right poles, respectively.
B. Comparison of model predictions in simulations with constant KMT half-life as used throughout this study (in green), and for the simulations in which KMT turnover was faster in prometaphase ($\tau_{1/2}$ = 3 min from 0 to 20 min) but then slowed down to $\tau_{1/2}$ = 6 min (in blue).
C. A layer containing two poles and a kinetochore pair for 2D model. Spindle MTs within this layer are shown in green; blue and red arrows depict forces acting on the kinetochore from the KMTs. Inset shows the enlarged kinetochore with three rotational axes. For more information see Supplement 1.2, section f.
D. Side view of the selected layer, which has thickness h_{kin}, which is chosen to equal the size of kinetochore; d is distance between the kinetochore and spindle pole; see Supplement 1.2, section f for details.
E. Same view as in panel D but showing chromosome rotation around X-axis (light blue). Note that such rotation reduces number of MTs that can bind to the kinetochore.

Supplemental Figure S2. Mechanics of chromosome motion and simulation algorithm.

A. Vector diagram of forces and velocities, see equations (s3 – s5). $\boldsymbol{V_c}$ – velocity of the center of mass of the chromosome; $\boldsymbol{r_i}$ – vector from the chromosome center of mass to the attachment point for KMT number i; $\boldsymbol{V_i}$ – velocity of the attachment point for KMT number i; $\boldsymbol{R_i}$ – unit vector from the attachment point of KMT number i to its corresponding pole; $\boldsymbol{F_i}$ – pulling force generated by KMT number i. Description of other symbols is provided in Supplement 1.4. For simplicity, only one spindle pole is shown.
B. Block scheme of the simulation algorithm, see Supplement 1.5.
C. Diagram illustrating the mechanism that causes orientation bi-stability in kinetochores with geometric constraints. Properly attached KMTs pull on the sister kinetochores toward opposite spindle poles, thereby orienting the kinetochore pair parallel to the spindle axis (upper schematics). If the kinetochore accidentally achieves the spindle-perpendicular orientation and the KMT connections are very stable, the kinetochore becomes trapped in this abnormal configuration because, as with proper orientation, all forces and torques are balanced (lower schematics).

Supplemental Figure S3. Additional modeling results.

A. Model features that accelerate the search and capture of a kinetochore. Acceleration factor (number above each column) was calculated relative to the simulations which lacked all these features. “10 μm spindle” results were compared to simulation with 20 μm spindle length; see Supplement 3.1.

B. The steady-state number of KMTs as a function of KMT half-life. Same data as in Figure 4A, but for a limited KMT half-life range to depict a linear fit.
C. Distributions of the number of MTs at kinetochore. Theoretical data (open bars) for PtK1 cells were obtained in the model using equation (s12) with the average number of KMTs 25; for human cells this number was assumed to be 18. Experimental data (closed bars) are from (McEwen *et al*., 1997, 2001).
D. Kinetics of different chromosome configurations in experiment (data from Figure 4D in (Silkworth *et al*., 2012)) and model predictions for $\tau_{1/2}$ = 6 min, N_{max} = 45. In the model, kinetochore with single inappropriate KMT was counted as bioriented.
E. Fraction of bioriented chromosomes at steady-state as a function of the rigidity of inter-kinetochore spring; $\tau_{1/2}$ = 6 min, N_{max} = 45.
F. Fraction of bioriented chromosomes as a function of the corona thickness; $\tau_{1/2}$ = 6 min, N_{max} = 45.

Supplemental Figure S4. Additional analysis of chromosome lagging and mis-segregation.

A. Probability to bind merotelic KMT at steady-state (i.e. metaphase) as a function of the steady-state number of KMTs; N_{max} = 45.
B. Percent of lagging chromosomes as a function of KMT half-life prior to anaphase. Chromosome was assumed to lag in anaphase if by the end of simulations its kinetochore had M/A > 0.5. Vertical gray bar indicates the physiological range for $\tau_{1/2}$ at metaphase; horizontal gray bar shows model predictions (2-8%) for this range; N_{max} = 45.
C. Probability to bind merotelic KMT at steady-state (i.e. metaphase) as a function of average M/A ratio; N_{max} = 45.
D. Average M/A ratio predicted for different KMT half-life at steady-state; N_{max} = 45.
E. Predicted mis-segregation rate per chromosome as a function of the number of "allowed" merotelic KMTs, i.e. merotelic KMTs that are assumed not to cause lagging but allow normal chromosome segregation in anaphase. N_{MT} is the average number of KMTs at steady-state (i.e. metaphase).

Supplemental references

Bakhoum SF, Thompson SL, Manning AL, Compton DA (2009). Genome stability is ensured by temporal control of kinetochore-microtubule dynamics. Nat Cell Biol., 11, 27-35.

Burns EM, Christopoulou L, Corish P, Tyler-Smith C (1999). Quantitative measurement of mammalian chromosome mitotic loss rates using the green fluorescent protein. J Cell Sci. 112, 2705-2714.

Ganem NJ, Godinho SA, Pellman D (2009). A mechanism linking extra centrosomes to chromosomal instability. Nature 460, 278-282.

Giodini A, Kallio MJ, Wall NR, Gorbsky GJ, Tognin S, Marchisio PC, Symons M, Altieri DC (2002). Regulation of microtubule stability and mitotic progression by survivin. Cancer Res. 62, 2462-2467.

Grishchuk EL, Molodtsov MI, Ataullakhanov FI, McIntosh JR (2005). Force production by disassembling microtubules. Nature 438, 384-388.

Mastro AM and Keith AD (1984). Diffusion in the aqueous compartment. J Cell Biol. 99, 180s-187s.

Mastronarde DN, McDonald KL, Ding R, McIntosh JR (1993). Interpolar spindle microtubules in PTK cells. J Cell Biol. 123, 1475-1489.

Minissi S, Degrassi F, Tanzarella C, Gustavino B (1999). Direct and indirect non-disjunction in the origin of trisomy in cultured human lymphocytes. Mutagenesis. 14, 557-562.

Nicholson JM and Cimini D (2013). Cancer karyotypes: survival of the fittest. Front Oncol. 3, 148.

Rusan NM, Fagerstrom CJ, Yvon A-MC, Wadsworth P (2001). Cell cycle-dependent changes in microtubule dynamics in living cells expressing green fluorescent protein-alpha tubulin. Mol Biol Cell 12, 971-980.

Toso A, Winter JR, Garrod AJ, Amaro AC, Meraldi P, McAinsh AD (2009) Kinetochore-generated pushing forces separate centrosomes during bipolar spindle assembly. J Cell Biol. 184, 365-372.

Wollman R, Cytrynbaum EN, Jones JT, Meyer T, Scholey JM, Mogilner A (2005) Efficient chromosome capture requires a bias in the 'search-and-capture' process during mitotic-spindle assembly. Curr Biol. 15, 828-832.

Wray W, Stubblefield E, Humphrey R (1972). Mammalian metaphase chromosomes with high molecular weight DNA isolated at pH 10.5. Nat New Biol. 238, 237-238.

Supplemental Table S1. Chromosome lagging and mis-segregation rates for different cell lines

"Normal" cells are more chromosomally stable than the "cancer" cell lines. When several references are available, mean values are used; errors are SEM; N/A – data not available. Lagging rate per chromosome (C^{lag}) was calculated from the percent of anaphases with lagging chromosomes (A^{lag}) and a modal chromosome number (N_{chrm}) using the following equation: $A^{lag}/100\% = 1-(1-C^{lag}/100\%)^{0.5N_{chrm}}$. ATCC refers to American Type Cell Culture website (www.atcc.org).

	Percent of anaphases with lagging chromosomes (A^{lag})	Modal chromosome number (N^{chrm})	Lagging rate per chromosome (C^{lag})	Mis-segregation rate per chromosome (C^{mis})	Mis-segregation to lagging rate ratio (100 C^{mis} / C^{lag})
NORMAL CELLS					
RPE-1	3.7 ± 1.2 % (Bakhoum et al., 2009a,b; Ganem et al., 2009)	46	0.15 %	1.9×10^{-4} (Thompson and Compton, 2008; Ganem et al., 2009)	0.12
human primary fibroblasts (MRC-5)	0.5 % (Cimini et al., 2002)	46	0.02 %	N/A	N/A
PtK1	1 % (Cimini et al., 2001)	12	0.16 %	8.5×10^{-4} (Salmon et al., 2005)	0.53
cultured human lymphocytes	0.36 % (Minissi et al., 1999)	46	0.016 %	N/A	N/A
BJ fibroblasts	0.8 ± 0.4 % (Ganem et al., 2009)	46	0.035 %	1.5×10^{-4} (Ganem et al., 2009)	0.43
isolated human hepatocytes	N/A	46	N/A	8.7×10^{-4} (Knouse et al., 2014)	N/A
isolated human brain cells	N/A	46	N/A	4.7×10^{-4} (Knouse et al., 2014)	N/A
CANCER CELLS					
HeLa	8 % (Nicholson and Cimini, 2013)	82 (Nicholson and Cimini, 2013)	0.2 %	2.1×10^{-3} (Burns et al., 1999)	1.05
HCT116	2.5 ± 0.5 % (Silkworth et al., 2009)	45 (Thompson and Compton, 2008)	0.11 %	2.5×10^{-4} (Thompson and Compton, 2008)	0.23
HT29	9 ± 1 % (Ganem et al., 2009; Silkworth et al., 2009)	68 ± 2 (Thompson and Compton, 2008)	0.27%	3×10^{-3} (Thompson and Compton, 2008)	1.11
U2OS	32 ± 6.4 % (Bakhoum et al., 2009b)	80 (Ganem et al., 2009a)	1.0 %	N/A	N/A
Caco2	39 ± 12 % (Ganem et al., 2009; Nicholson and Cimini, 2013)	87 ± 9 (Thompson and Compton, 2008)	1.2 %	9×10^{-3} (Thompson and Compton, 2008)	0.75
MCF-7	26 ± 9 % (Bakhoum et al., 2009a; Ganem et al., 2009; Nicholson and Cimini, 2013)	78 ± 3 (Thompson and Compton, 2008)	0.7 %	7.5×10^{-3} (Thompson and Compton, 2008)	1.1
U251	16 ± 2.0 % (Bakhoum et al., 2009b)	N/A	N/A	N/A	N/A
U87	19.3 ± 2.0 % (Bakhoum et al.,	44 (ATCC)	0.95 %	N/A	N/A

	2009b)				
DAOY	36.7 ± 1.8 % (Bakhoum et al., 2009b)	96 (ATCC)	0.95 %	N/A	N/A
U118	50.0 ± 6.4 % (Bakhoum et al., 2009b)	N/A	N/A	N/A	N/A
BT-549	12 ± 3 % (Ganem et al., 2009)	78 (Nicholson and Cimini, 2013)	0.33 %	N/A	N/A
MDA-231	12 ± 3 % (Ganem et al., 2009)	64 (Nicholson and Cimini, 2013)	0.4 %	N/A	N/A
SCC114	7 ± 3 % (Ganem et al., 2009)	N/A	N/A	N/A	N/A
CFPAC-1	9 ± 3 % (Ganem et al., 2009)	73 (Nicholson and Cimini, 2013)	0.26 %	N/A	N/A
SW620	7 ± 1 % (Ganem et al., 2009)	50 (Nicholson and Cimini, 2013)	0.3 %	N/A	N/A

Supplemental Table S2. Symbols used in the model. n/a – not applicable.

Symbols	Description	Value, units	Reference
Spindle structure			
n/a	Spindle length, i.e. distance between two poles at maximum separation	10 µm	Mastronarde *et al*., 1993; Giodini *et al*., 2002
n/a	Total number of dynamic microtubules (MTs) per pole	750	McIntosh and Landis, 1971
n/a	Time of the spindle poles separation	120 s	Toso *et al*., 2009
MT dynamics			
V_{pol}	Rate of MT polymerization	12.8 µm/min	Rusan *et al*., 2001
V_{dep}	Rate of MT depolymerization	14.1 µm/min	Rusan *et al*., 2001
f_{cat}	Catastrophe frequency	0.058 s^{-1}	Rusan *et al*., 2001
f_{res}	Rescue frequency	0.045 s^{-1}	Rusan *et al*., 2001
Kinetochore structure and motion			
R_{chrom}	Radius of the half-cylinder that represents a primary constriction	0.3 µm	Ris and Witt, 1981
L_k	Resting length of the inter-kinetochore spring (between sister kinetochores)	0.8 µm	Loncarek *et al.*, 2007
L_c	Radius of the kinetochore	0.25 µm	Ris and Witt, 1981
l_c	Thickness of kinetochore corona	100 nm	Cheeseman and Desai, 2008
k_{kin}	Rigidity of the inter-kinetochore spring	1.4 pN/nm	Supplement 1
ψ	Angle between the spindle and kinetochore axes as a function of simulation time	model variable	n/a
M	Chromosome mass	10^8 Da	Wray *et al*., 1972
γ (η)	Chromosome friction drag coefficient for translational (rotational) motion	6×10^{-3} pN s/nm (10^3 pN nm s/rad)	Nicklas, 1965
D_{chrom}	Free chromosome diffusion coefficient	10^{-11} cm^2 /s	Supplement 1

Kinetochore-MT interactions			
N_{max}	Maximum number of KMTs at one sister kinetochore	45	McEwen *et al*., 1997
N_{MT}	Number of KMTs per sister kinetochore as a function of simulation time	model variable	n/a
k_{det}	Detachment rate for KMT (i.e. $\ln 2/\tau_{1/2}$, where $\tau_{1/2}$ is average KMT half-life)	as defined by the KMT half-life	n/a
A	Maximum force produced by one KMT	45 pN	Grishchuk *et al*., 2005
b	Slope of the force-velocity curve for depolymerizing MT (= A/V_{pol})	3.2 pN min/µm	n/a
Other parameters			
T	Ambient temperature	300 K	current model
dt	Time step	0.3 s	current model

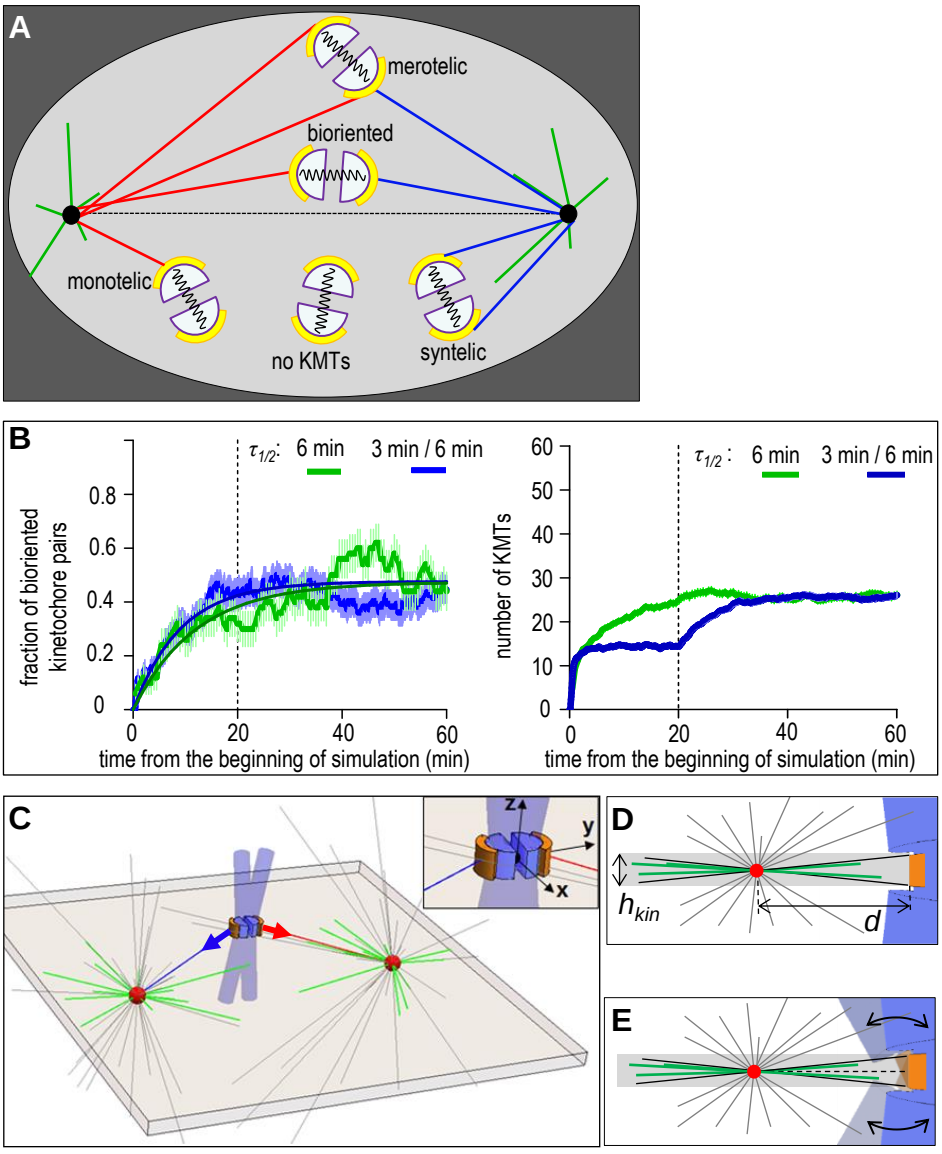

Supplemental Figure S1

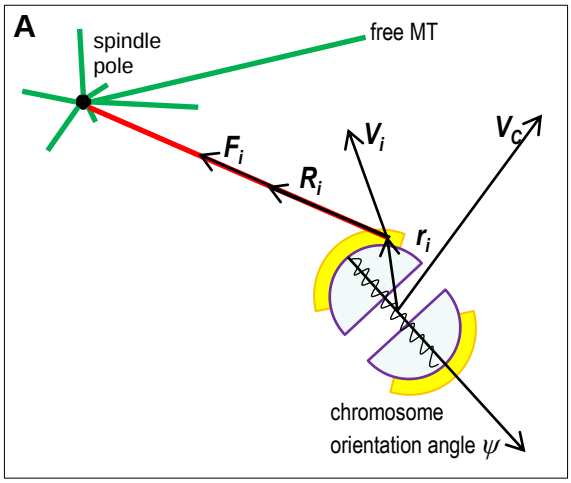

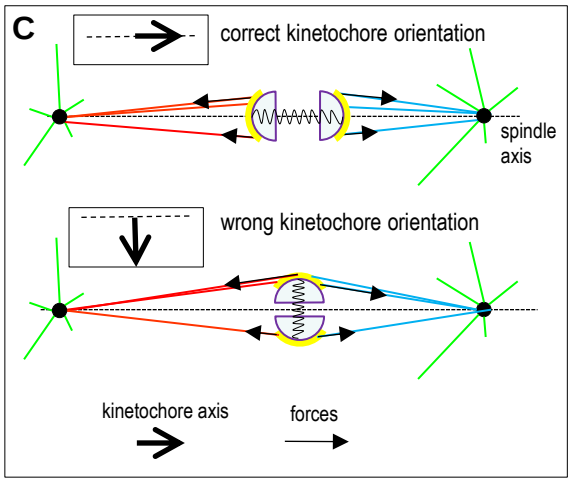

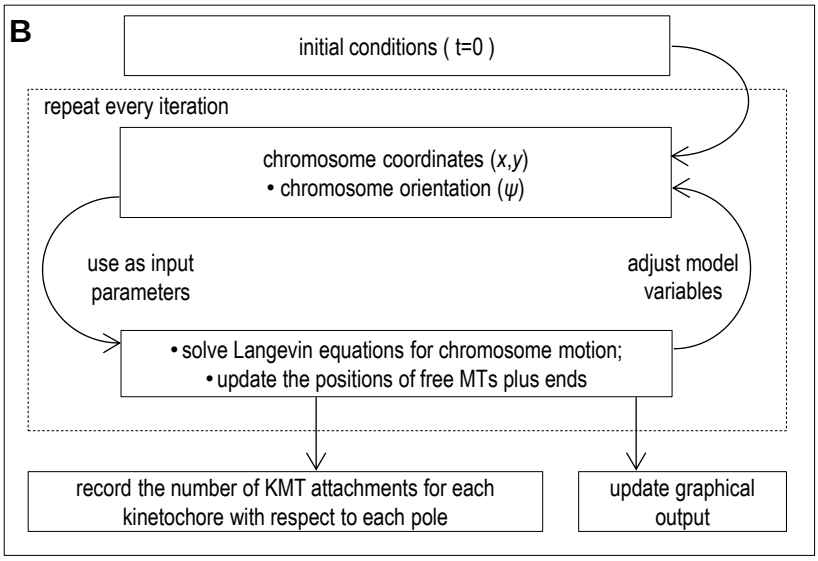

Supplemental Figure S2

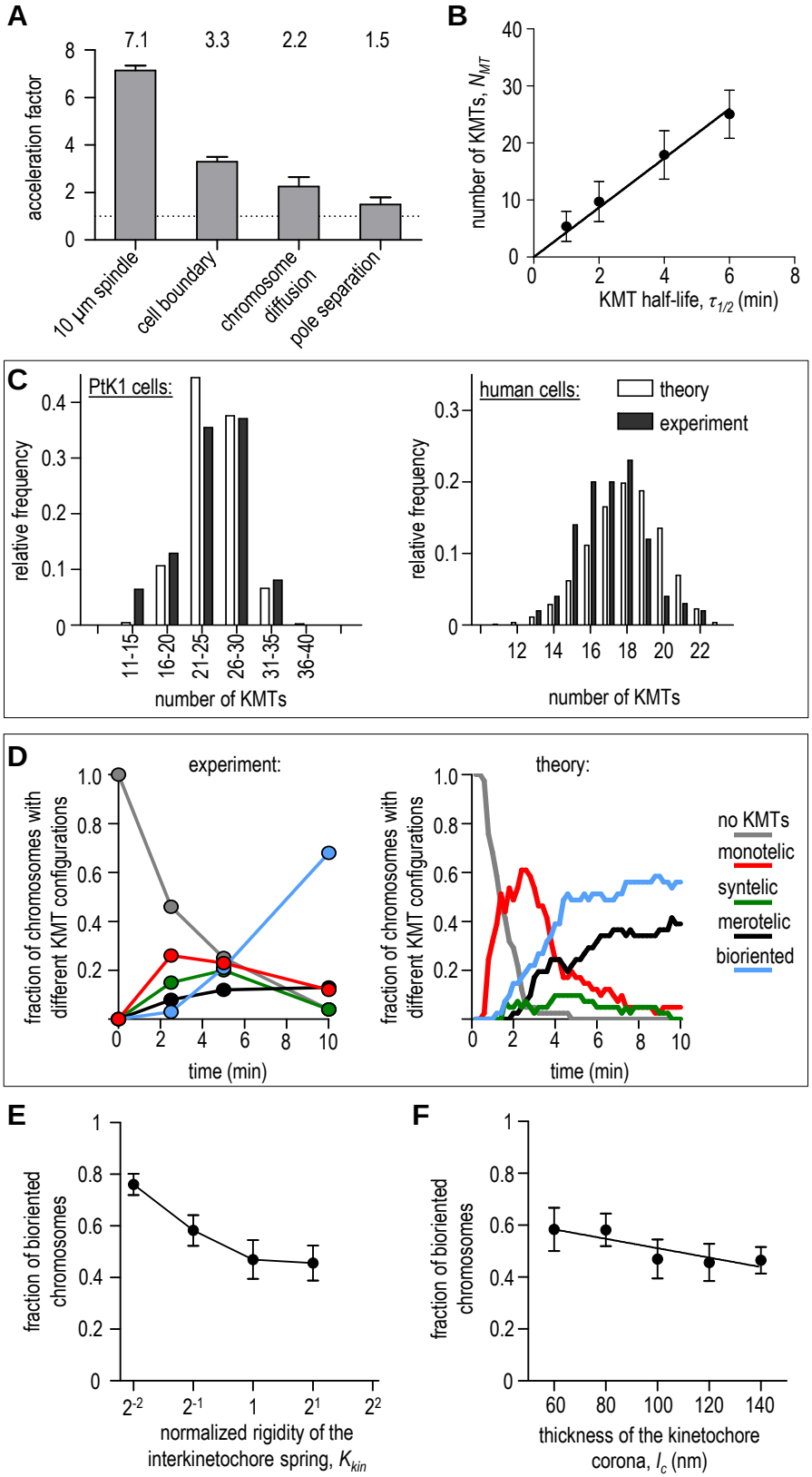

Supplemental Figure S3

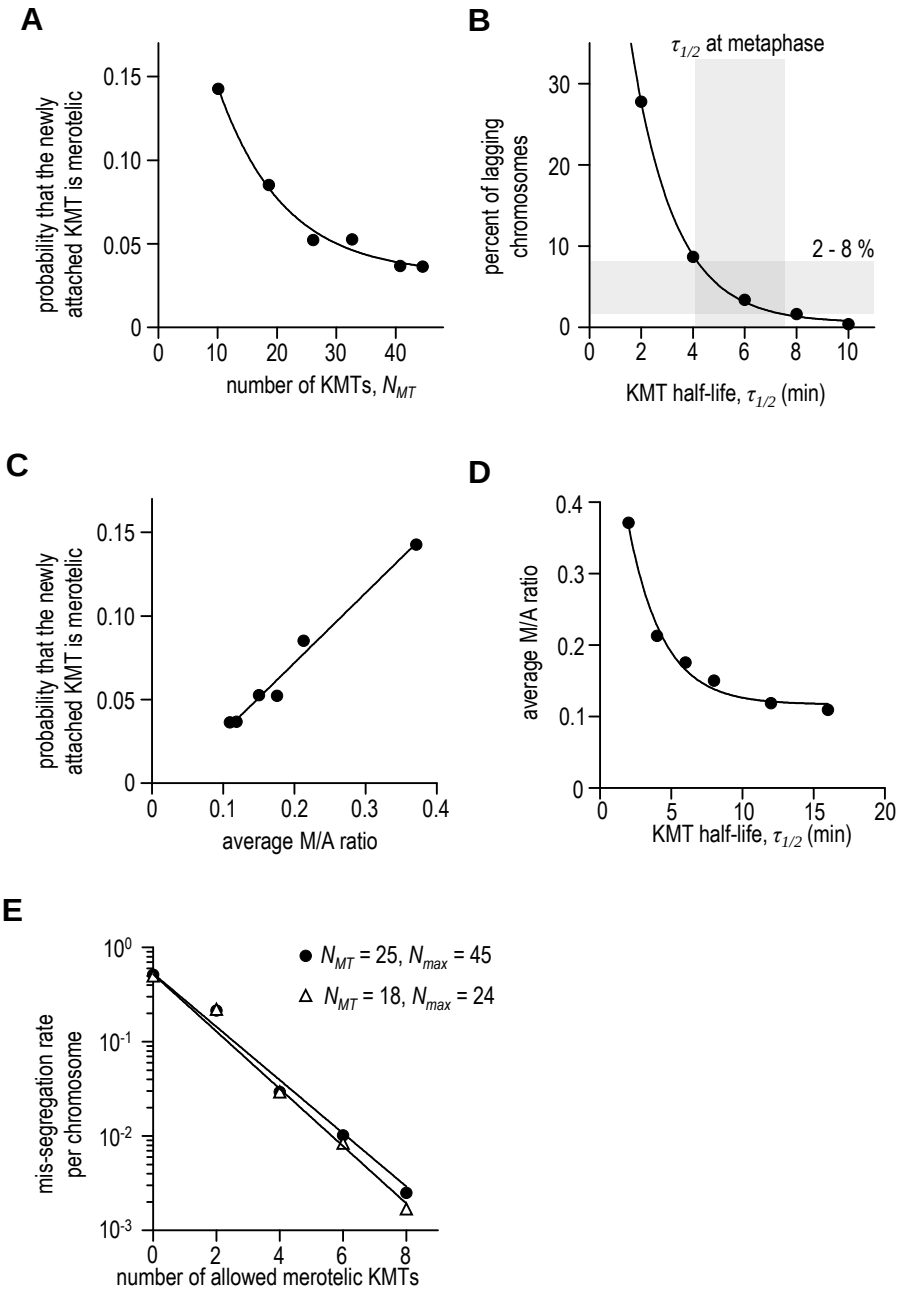

Supplemental Figure S4